Int. J. Heat Mass Transfer. Vol. 31, No. 12, pp. 2559–2570, 1988
Printed in Great Britain

0017–9310/88 $3.00 + 0.00

Two-phase flow regime transition criteria in post-dryout region based on flow visualization experiments

N. T. OBOT
Department of Chemical Engineering, Clarkson University, Potsdam, NY 13676, U.S.A.

and

M. ISHII†
Reactor Analysis and Safety Division, Argonne National Laboratory, Argonne, IL 60439, U.S.A.

(*Received* 10 *December* 1987 *and in final form* 2 *May* 1988)

Abstract—A visual study of film boiling is carried out to determine the flow regime transition in the post-CHF region. An idealized inverted annular flow is obtained by introducing a liquid jet of Freon 113 through a nozzle, precisely centered with respect to the internal diameter of the test section, with an annular gas flow. The respective ranges for liquid and gas velocities are 0.05–0.5 and 0.03–8.2 m s^{-1}. Nitrogen and helium are used in the study. For the present configuration, there are four flow regimes; namely, the smooth inverted annular flow section, the rough wavy, agitated and dispersed flow regimes.

1. INTRODUCTION

AN INVERTED annular flow, which consists of a liquid core surrounded by a vapor annulus, is of considerable importance in the areas of light water reactor (LWR) accident analysis, cryogenic heat transfer, and other confined, low quality film boiling applications. Although extensive studies of the heat transfer characteristics for this flow situation have been carried out by numerous researchers [1–3], there have been very few systematic investigations of the hydrodynamics of inverted annular flow.

An understanding of the effects of the various parameters on the prevailing local flow conditions in the post-CHF region (such as, the shape of the liquid/vapor interface, the stability as well as the disintegration of the liquid core) is of fundamental importance in flow modeling and development of predictive equations for interfacial transfer rates. Realizing that in typical film boiling experiments, control of test conditions as well as direct measurements of the pertinent flow parameters, that would be needed for such an understanding, are quite difficult, the recourse must be to devise simplified experiments.

The main objective of the inverted annular flow research program was to determine the effects of inlet liquid and gas conditions on the flow regimes in the post-CHF region. A flow visualization of a simplified film boiling configuration, consisting of a Freon 113 liquid core surrounded by a gas annulus, was made. From an analysis of the still photographs and high-speed motion pictures, it was determined that there are basically four flow regimes and it was also possible to determine the axial extents of these flow zones with remarkable consistency. Predictive equations, in generalized and simplified forms, were then developed for the axial limits of the different flow regimes.

2. REVIEW OF EXPERIMENTAL STUDIES OF POST-CHF REGION

Most of the research on the post-CHF region dealt mainly with heat transfer. Excellent reviews of the widespread literature were provided by Jordan [1] and Clemments and Colver [2]. A subsequent review by Kalinin *et al.* [3] considered both free and forced convective film boiling in great detail. Complete tabulations as well as extensive graphical comparisons of the various predictive equations for heat transfer were given. However, because heat transfer or hydraulic resistance is significantly influenced by the regime of film boiling, some of the disagreement among the various correlations are not so readily explained due to insufficient understanding of the complex hydrodynamics of the post-CHF region.

Visual and high-speed motion picture observations of film boiling in channels have been reported by a number of researchers. For example, Chi and coworkers [4–6] considered film boiling of saturated hydrogen under transient cooling conditions and obtained the following flow regimes along the horizontal test section: annular, slug and dispersed flows. For the range of flow conditions covered in their study, Kalinin *et al.* [7] observed both the annular and slug flow regimes.

For upward flow of liquid nitrogen in a vertical tube, Laverty and Rohsenow [8] obtained two distinct flow regimes: an annular flow with liquid in the center

† Present address: School of Nuclear Engineering, Purdue University, West Lafayette, IN 47907, U.S.A.

NOMENCLATURE

A_i	constant, defined by equation (3)
B_i	constant, defined by equation (4)
C_i	constant, defined by equation (6)
Ca	capillary number, $\mu_f v_f/\sigma_f$
D_j	liquid jet hole diameter [m]
L	distance measured from nozzle exit (test section entrance) [m]
L_B	mean axial extent of a flow section [m]
Re	Reynolds number, $\rho V D_j/\mu$
V	velocity [m s^{-1}]
V_{rel}	relative velocity, $V_g - V_f$ [m s^{-1}]
We	Weber number, $\rho V^2 D_j/\sigma$
$We_{g,rel}$	gas Weber number, $\rho_g V_{rel}^2 D_j/\sigma_f$.

Greek symbols

α	void fraction at inlet to test section
μ	viscosity [Pa s]
ρ	density [kg m^{-3}]
σ	surface tension [N m^{-1}].

Subscripts

f	liquid
g	gas
j	liquid jet
rel	relative, or based on V_{rel}.

and vapor in the annulus occurred at the beginning of the heated section, followed by a dispersed region of filaments/droplets of liquids at greater tube lengths. In a subsequent study, Forslund and Rohsenow [9] confirmed the large departure from thermal equilibrium in the dispersed flow film boiling.

A detailed experimental study of adiabatic inverted annular flow was carried out by DeJarlais [10], DeJarlais *et al.* [11], and Ishii and DeJarlais [12] using coaxial downward flow water jets and various gases in a glass tube. The disintegration of the liquid core into droplets was found to be due to two different mechanisms: wave instabilities at the interface and roll-wave entrainment. Correlations for core shape, breakup mechanisms and dispersed core drop size were developed, by extending the results of free jet instability, roll-wave entrainment and churn turbulent droplet stability studies.

Since the absence of film boiling conditions (no wall wetting, droplet vaporization in the vicinity of a heated wall, etc.) may limit the applicability of the adiabatic results, an extensive and consistent flow visualization study of a diabatic inverted annular flow was performed by DeJarlais and Ishii [13–15]. A simplified upward flow geometry, consisting of a liquid jet of Freon 113 surrounded by a gas annulus, was studied. In addition to the existence of an annular and dispersed flow regime, in line with the results of Laverty and Rohsenow [8], the presence of two well-defined regimes—the agitated and the inverted slug/churn flow—was also documented. The axial extent of each flow regime, as well as the transition from one regime to another, was found to depend markedly on the relative velocity between the gas and the liquid, in agreement with the observation of Laverty and Rohsenow. No correlations were developed for the extents of the flow regimes.

The channel flow film boiling studies reviewed so far dealt almost exclusively with visual, still and movie-camera observations of the complete structure of the two-phase flow field. Although it has long been known that the prevailing film boiling regime has profound effects on heat transfer and on the hydraulic resistance, only several studies of film boiling hydraulic resistance have been reported (Kalinin *et al.* [7], and Graham *et al.* [16]). Also, there is almost no systematic study of the rather complicated void fraction distribution for film boiling in channels for a range of inlet flow conditions. Ottosen [17] obtained void fraction data using a γ-ray adsorption technique in the flow visualization experiments in a vertical glass tube with liquid nitrogen as a coolant. He noted that the transition from an annular to a dispersed flow occurred at void fractions in excess of 80% at atmospheric pressure. Kurilenko *et al.* [18] made measurements of void fraction by the radioisotope method using vertical and downward flow transient quenching of a steel tube with liquid nitrogen, but the scope of the study was quite limited.

Although some progress has been made in the identification of the various flow regimes, as reflected here by the findings of previous investigators, the general state of knowledge of the detailed structure and mechanisms of two-phase flows for film boiling has not been entirely satisfactory. Comprehensive experimental investigations of these complex hydrodynamics of the post-CHF region are certainly needed in order to provide data for further development of theoretical models.

The emphasis in this brief review has been on the experimental studies. It should also be mentioned that a number of computer codes and analytical/empirical models have been developed for predictions of void fractions, wall temperatures and heat fluxes in the post-CHF region [19, 20]. A review of the numerous analytical and empirical methods for annular and slug flow film boiling was carried out by Groeneveld [21] while Chen [22], in his review, examined phenomenological questions relevant to our understanding of the transport mechanisms in the post-CHF heat transfer. More recently, Yadigaroglu and Bensalem [23] presented a critical and thorough review of the

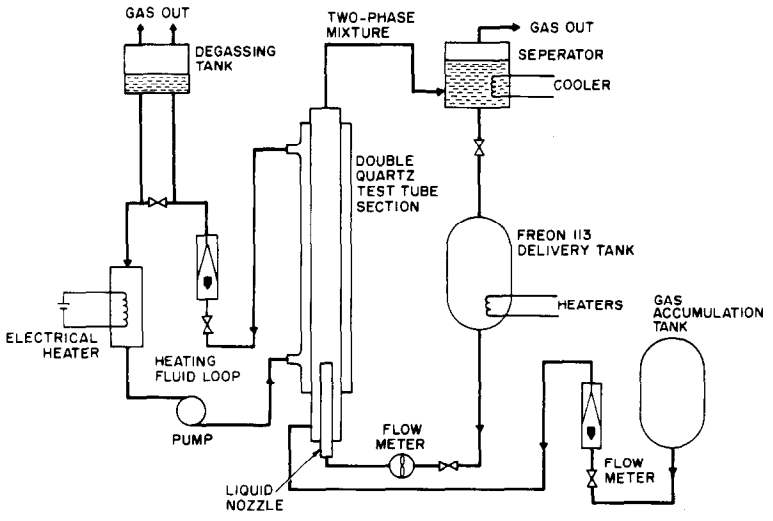

FIG. 1. Schematic of the experimental facility.

various approaches that are used for modeling of interfacial mass generation in two-phase flows, including a detailed discussion of the mechanistic models for inverted annular and dispersed flow film boiling. A common conclusion that can be inferred from these reviews amounted to this: there is need for experimental data base that would permit validation of the existing models as well as development of improved models.

3. EXPERIMENTAL FACILITY AND TEST PROCEDURES

3.1. *Test apparatus*

The steady state film boiling experimental facility, shown schematically in Fig. 1, consisted of a transparent quartz tube, a simplified inverted annular flow geometry formed by a round liquid jet core surrounded by an annular gas flow. The liquid jet of Freon 113 was discharged into the test section using thin-walled interchangeable stainless steel tubes (9.02 and 10.8 mm i.d.), each of which was precisely centered with respect to the internal diameter of the heated quartz tube, while the gas (nitrogen or helium) was introduced via the annular gap between the stainless steel nozzle and the quartz tube. The corresponding void fractions were 0.56 and 0.37 for $D_j = 9.02$ and 10.8 mm, respectively. Liquid and gas flow rates were measured with turbine flowmeter and rotameters, respectively; temperatures at all critical locations being sensed with chromel–alumel thermocouples.

The heated portion of the test section, 1.0 m in length (Fig. 2), consisted of two quartz tubes, finished in much the same way as Liebig or West condensers. The dimensions of the inner and outer quartz tubes were 16×13.6 mm o.d./i.d. and 35×31 mm o.d./i.d., respectively, giving an annular gap of 31×16 mm o.d./i.d. through which a high temperature heat transfer fluid (Syltherm 80 by Dow Corning, Midland, Michigan) was circulated. The inner quartz tube extended beyond the outer one to give an unheated entrance length of 150 mm (Fig. 2).

Inverted annular flow could be established in the test section by heating the heat transfer fluid above the minimum film boiling temperature and then introducing saturated or subcooled test liquids such as Freon 113 into the inner tube directly. The drawback with this approach is one of lack of control of the annular gas conditions. The alternative simplified inverted annular flow geometry, one that was used for the present study and afforded accurate control of the flow conditions at the inlet to the test section, was obtained by introducing a circular liquid jet through the stainless steel tube with a surrounding annular gas flow (Figs. 1 and 2), the latter being discharged through an annular plenum located below the quartz test section.

3.2. *Test procedures, photographic technique and data analysis*

Preliminary preparations prior to a trial run included degassing of the Freon supply tank and the establishment of the desired Freon temperature by heating and/or cooling, charging of the gas accumulation tank to 60–80 psig, heating of the Syltherm loop to a stable temperature of 225–270°C, cooling of the separator tank (used to recover the Freon from a two-phase mixture leaving the test section) to about 0°C or lower, and a check on the lighting conditions to be used for photographic and/or motion picture observations. In these experiments, the gas was at room temperature, between 22 and 27°C, depending on the trial run. The Freon temperature, prior to delivery to the test section, was also within the above range.

During a trial run, visualization of the hydrodynamic behavior within the test section was

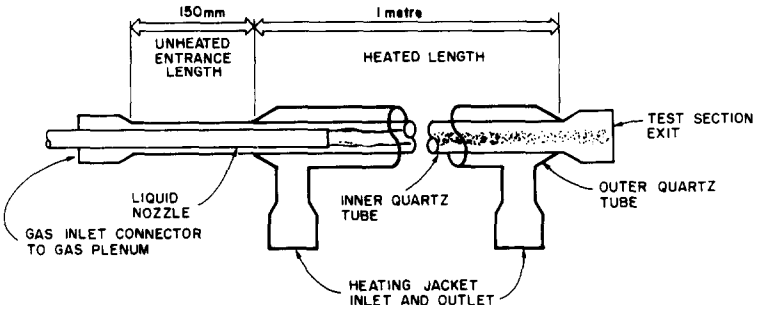

FIG. 2. Details of the test section.

accomplished using both still photographs and high-speed motion pictures. For the former, a 35 mm SLR camera was used along with 400 ASA black and white film. Lighting was provided by either of two 3 μs strobe lights, each delivering a 0.5 W s pulse of light. With this short exposure time, small (0.1 mm) droplets traveling at speeds above 10 m s^{-1} were observed without significant blurring of the image. The light from the strobe was bounced off a white background onto the test section.

For a given test run, a series of still photographs were taken using a 55 mm lens which provided a complete view of a 0.3 m length of the test section on each 35 mm film frame. The pictures were taken at five or six locations, spanning the full length of the test section, including the entrance and exit sections. At each location, two to five photographs were taken, giving about 10–30 frames for each trial. To obtain a more detailed structure of the flow field, additional still photographs were taken with 105 or 200 mm lenses. Either back or side strobe lighting was used.

For some selected trials, motion pictures were taken using several different cameras and Kodak VNX 430 (400 ASA) color reversal film, with a film speed of 500 fps for most trials. Lighting was provided by four 450 W floodlights, these being directed onto the same background as noted above for the still photographs. The interested reader may wish to refer to the detailed discussion of the qualification methods for optical and/or photographic techniques which is given in ref. [13].

The last comment here deals with the data used to generate the correlations shown subsequently. These were obtained by analyzing the still photographs, taken with the 35 mm black and white film, in the following manner. The axial extents of the different flow regions were established by carefully studying the developed negatives using a light table fitted with a binocular microscope, the reference scale being the image of the graduated scale (in cm) mounted alongside the test section. Liquid surface tension data used for computation of Weber numbers were obtained from Sinitsyn *et al.* [24]. For drop size analysis, the negatives obtained with the 55 mm SLR lens were projected onto a screen, with a minimum negative-to-screen image magnification of 500. By this procedure the drop sizes were determined down to the 100–200 μm size range. Although determination of the flow regime or the sizes of the droplets were accomplished with little difficulty, a shortcoming is the rather time consuming frame by frame analysis. Motion pictures of the flow field were analyzed on a motion picture analyzer, with x–y plotting cross hairs and film projection speeds from 48 fps down to zero.

4. RESULTS AND DISCUSSION

4.1. *An overview of the hydrodynamics of the flow field*

Prior to presentation and discussion of the results for the axial extent of the flow regimes, it is instructive to review the flow patterns that were established for this simplified inverted annular flow. This brief summary is intended to provide the reader with a clear picture of the most important characteristics of the various flow regimes, and will not contain exhaustive details.

4.1.1. *Smooth (small surface wave) section.* This smooth region begins from the nozzle exit (test section entrance) and can extend to about 30 nozzle diameters depending, of course, on the relative velocity between the gas and the liquid core. For a given liquid jet entrance velocity, the maximum length occurs at very low gas exit velocities, decreasing markedly with increasing gas velocity to almost zero at high gas velocities. The shearing effect on the liquid jet by the gas; notably, the complete elimination of a smooth section as observed in the present study at high gas velocities, parallels that usually encountered in twin fluid atomization processes.

4.1.2. *Rough wavy section.* With increasing distance downstream, the liquid interface becomes wavy with nearly symmetric waves, the wavelengths of which are roughly 10 mm (order of magnitude). Except for the existence of a rough wavy interface, this region of the flow field is quite solid, with a fairly intact liquid core filling the center of the test section. As with the smooth section its axial extent varies according to whether the gas velocity is greater or less than the liquid jet velocity. For example, with V_{rel} (i.e. $V_g - V_f$) > 0, the

physical length of this flow regime decreases (from about 10–20 nozzle diameters) with increasing V_{rel} to the point that, at a V_{rel} of about 2 m s^{-1}, both the smooth and rough wavy sections are nonexistent, the prevailing regimes being an agitated zone in the immediate vicinity of the nozzle exit and large liquid slugs/ligaments over the remaining portion of the test section. By contrast, test trials with $V_{rel} < 0$ resulted in lengths that were within 10–50 jet hole diameters. It is pertinent to note that in DeJarlais and Ishii [13–15], this regime is referred to as the agitated solid core while the present agitated section, to be discussed next, corresponds to the inverted slug/churn flow in refs. [13–15].

4.1.3. *Agitated section.* With increasing downstream distance and/or at sufficiently high gas velocity, the nearly axisymmetric interfacial waves become very irregular and transform to large amplitude or roll-waves. Further from the rough wavy section or at a still larger gas velocity, significant interfacial deformation occurs, resulting in the break-up of portions of the roll-waves into ligaments and droplets. This mechanism of liquid break-up or drop formation has been treated quite well by Ishii and Grolmes [25] and DeJarlais [10], hence the details will not be given here. Other general features of this flow regime include the formation of skirt-like annular sheets of liquid due to extreme growth and distortion of the roll-waves, the presence of a highly agitated liquid annulus in the vicinity of the heated wall and of large liquid slugs in the central portion of the test section. With these general characteristics, it is quite clear that, unlike the smooth or rough wavy section, this section of the flow which may extend beyond the end of the heated portion of the test section (depending on the liquid and gas flow rates) is very unstable.

4.1.4. *Dispersed (ligament and drop) section.* For the ranges of liquid and gas velocities covered in the present study, this flow regime was generally confined to the downstream locations nearest to the test section exit. For test trials with high relative velocities, i.e. $(V_g - V_f) > 1$ m s^{-1}, the dominant feature of the downstream flow field was that of dispersed ligaments/droplets with either of the gas species. For low-to-moderate V_{rel} values, many of the large liquid ligaments or slugs at the exit of the test section were very distorted. If the test section were sufficiently long, it is likely that these ligaments would eventually disintegrate into smaller, stable drops.

4.1.5. *Photographic illustrations.* To shed some light on the general features outlined above, close-up photographs for a typical trial with nitrogen is given on Fig. 3. The respective values for liquid and gas velocity were 0.17 and 0.30 m s^{-1}, and the Freon temperature was 23°C. On this figure the test section entrance begins at $L = 0$ and with increasing number on the scale one is moving downstream towards the exit. Figure 3 shows that a fairly intact liquid core, with a surrounding annular gas flow, extends from $L = 0$ to about 30 cm. Of this initial length, the smooth section is no more than 3 cm while the remaining is essentially the rough wavy section. The general structure of the agitated region is also clearly in evidence beginning from about $L = 30$ cm. With increasing distance downstream it is especially noticeable that the core becomes quite agitated, with a fine interfacial structure consisting of liquid ligaments and droplets. Some of these details are beyond the optical limits of the present photographic equipment; notably for the $L = 65$–75 cm region where droplets of sizes smaller than 25–50 μm are discernible.

4.2. *Formulation of the generalized correlations*

From a detailed study of an adiabatic inverted annular flow [10–12], it was established conclusively that the correlated jet break-up data followed two distinct trends; one for the region over which the jet break-up length was independent of void fraction, relative velocity or gas density, with a marked sensitivity of the break-up to these variables for the second region. The break-up lengths for these two regions were closely approximated by the following equations:

$$L_B/D_j = 480 Re_j^{-0.53} We_j^{0.5} \quad (1)$$

$$L_B/D_j = 685 Re_j^{-0.53} We_j^{0.5} [We_{g,rel}/\alpha^2]^{-0.645}. \quad (2)$$

Since the two curves intersect at $We_{g,rel}/\alpha^2 = 1.73$, this critical value of the modified Weber number provides a useful criterion for determining the validity range for each equation. Another important finding was that the break-up mechanisms for an adiabatic inverted annular flow were similar to those documented in the literature for free jets.

On the basis of the above information, it was envisaged that the average extent of each flow regime could be correlated in terms of the non-dimensional variables in equations (1) and (2). Accordingly, the present data were reduced and the results are presented graphically in Figs. 4–7. The first three figures show, successively, the mean axial extents for the smooth, rough wavy and agitated flow sections. Beyond the agitated flow regime lies the dispersed ligaments/droplets section. The extent of this zone is shown in Fig. 7 from which it may be noted that it extends beyond the heated portion of the test section for most trials. The data used to prepare these plots are presented in tabular form in ref. [26].

In each of Figs. 4–7, data are shown for the two gas species (helium and nitrogen) tested. To provide useful insight on the role of relative velocity, it was considered worthwhile to further identify the data points in Figs. 4–6 according to whether the average gas velocity at the annulus (V_g) is less or greater than the liquid jet velocity (V_f) at the inlet to the test section.

Another general comment, one that is of particular importance, relates to the interpretation of the data for L_B/D_j. Each value of L_B, always measured from the nozzle exit (test section entrance), is scaled with

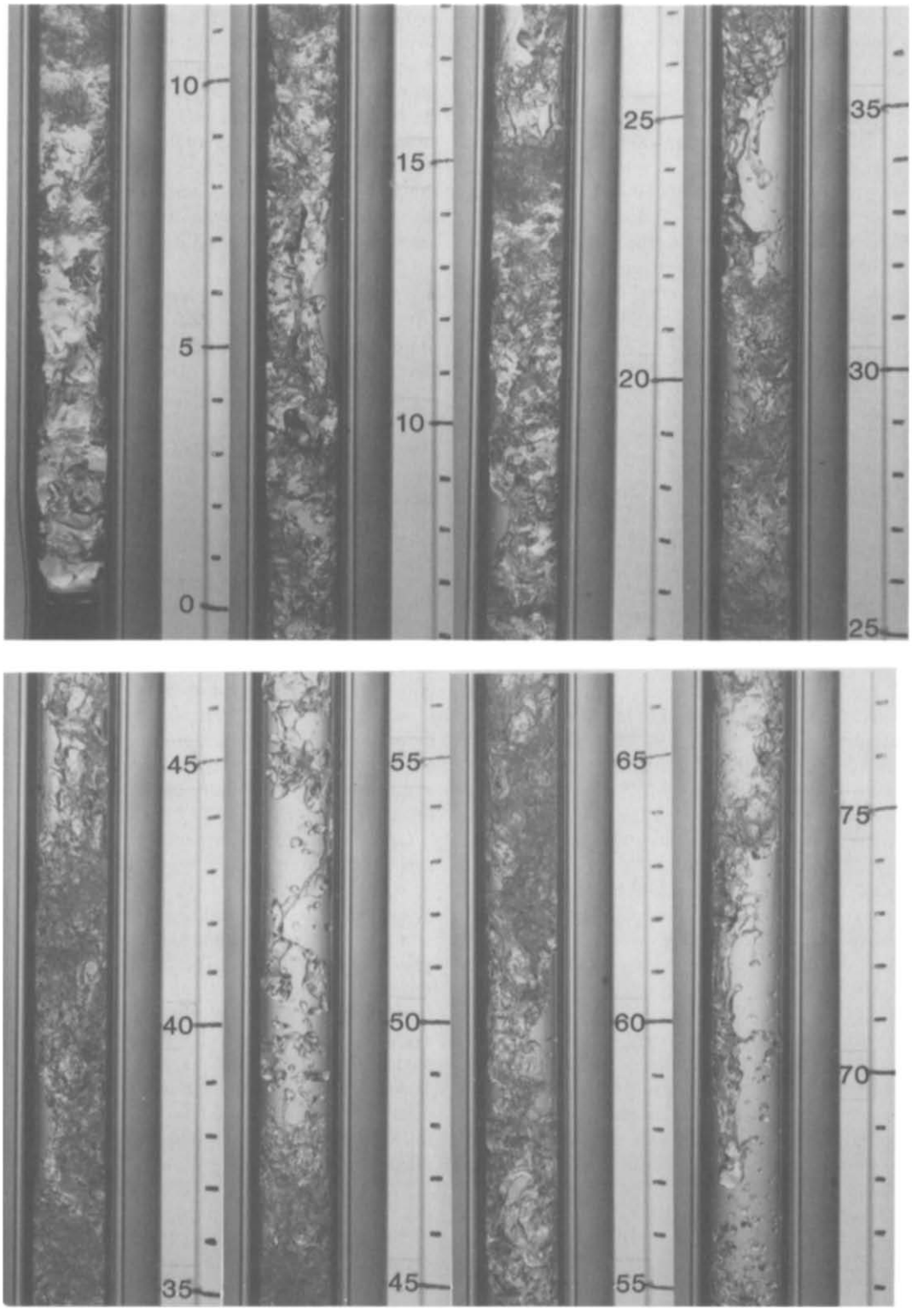

Fig. 3. Close-up photographs with nitrogen with $V_f = 0.17$ m s^{-1} and $V_g = 0.30$ m s^{-1}.

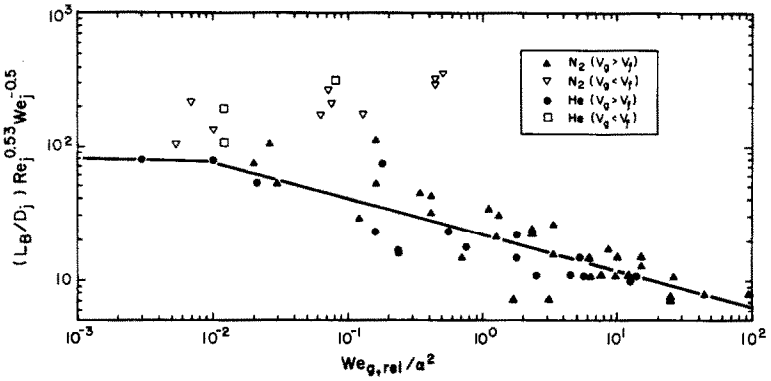

FIG. 4. Correlation for average length of smooth flow section.

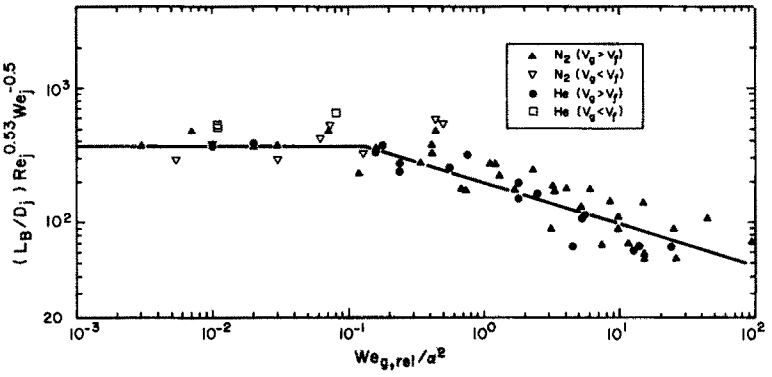

FIG. 5. Correlation for average length of rough wavy section.

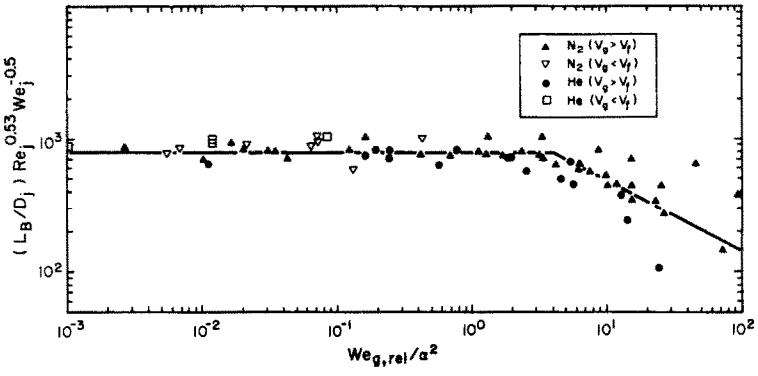

FIG. 6. Correlation for average length of agitated section.

the constant nozzle diameter, D_j. Thus, depending on the liquid and gas velocity, the observed average length, L_B/D_j, for the rough wavy section includes that for the smooth region, while that for the agitated regime may include both the smooth and rough wavy regions. Likewise, the L_B/D_j value for the dispersed zone may encompass all or some of those for the preceding upstream regimes. Given the fluctuating nature of the agitated region (due mainly to chugging), the fact that even under steady inlet flow conditions the flow in the test section is inherently unstable and changes from frame to frame, and difficulties associated with precise determination of the regime boundaries, the data that are given in Figs. 4–7 represent average values obtained by studying the 16–20 photographic frames taken for a given set of inlet flow conditions.

The general trends on Figs. 4–7 are twofold; a nearly constant L_B/D_j value with increasing $We_{g,rel}/\alpha^2$ for the region over which the average limits depend solely on the inlet liquid jet conditions, Re_j and We_j, followed by steadily decreasing values with further

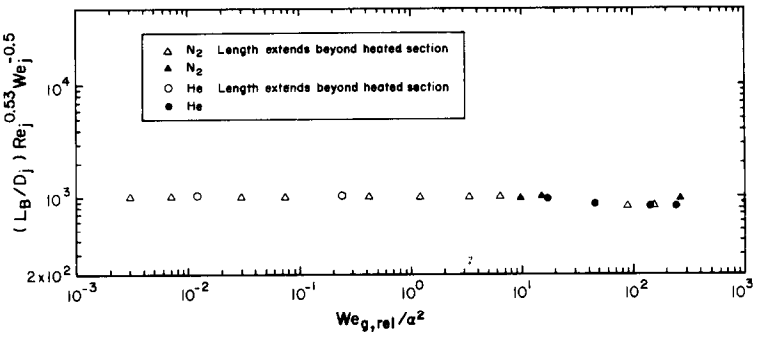

FIG. 7. Typical extent of dispersed flow section.

increases in $We_{g,rel}/\alpha^2$, which is the expected trend when L_B/D_j is dependent on both liquid and gas conditions at the inlet to the test section. For the smooth section, the length of which exhibits the greatest sensitivity to variations in relative velocity, gas density and void fraction, the few data available [26] for $We_{g,rel}/\alpha^2 < 10^{-3}$ together with those shown in Fig. 4 favor the observation that this extent is essentially independent of gas Weber number for $We_{g,rel}/\alpha^2 < 10^{-2}$.

An exception to the trends noted above is observed to occur for the dispersed flow section (Fig. 7). Here, it will be noted that, over the entire $10^{-3} \leqslant We_{g,rel}/\alpha^2 \leqslant 10^3$ range, L_B/D_j is almost determined solely by the liquid jet Reynolds and Weber numbers, Re_j and We_j. Conceivably, with increasing modified gas Weber number, conditions would eventually have been obtained for which L_B/D_j would decrease markedly with $We_{g,rel}/\alpha^2$, in line with the trends on Figs. 4–6. The general trend on this figure appears to support this view.

To render the results on Fig. 7 intelligible, it is necessary to discuss briefly the test conditions and the attendant flow phenomena. For the nitrogen trials, two values of liquid velocity (0.34 and 0.5 m s^{-1}) were used, while the annular gas velocity was varied between 0.52 and 8.2 m s^{-1}. For $V_f = 0.5$ m s^{-1} and $V_g = 0.52$ m s^{-1}, the average limits for the smooth, rough wavy and agitated section were $2D_j$, $15D_j$ and $70D_j$, successively, while the region of dispersed flow extended beyond the heated section beginning from about $70D_j$. Although the axial extents of the first three regions decreased markedly with almost complete depletion of the smooth zone, while the dispersed region increased, as the gas velocity was progressively increased, the latter continued to extend beyond the heated section up to $V_g \approx 4.4$ m s^{-1}. These results are so identified in Fig. 7 and, for these trials, only portions of this zone (up to the end of the heated section) were measured. For $V_g > 4.4$ m s^{-1}, the prevailing flow in well over two-thirds of the test section was one of dispersed droplets, with flaky remnants towards the exit of the test section, and these results are indicated with solid symbols. For these trials with high gas velocities, the dominant feature was liquid atomization into droplets in the vicinity of the test section entrance, and there was almost complete vaporization of the drops prior to the exit of the test section. For the helium trials, V_f was held constant at 0.34 m s^{-1} while V_g was varied between 0.22 and 5.6 m s^{-1}. These results have also been classified accordingly.

A closer examination of the results in Figs. 4–6 reveals one consistent trend with test trials for which the liquid jet velocities were larger than the annular gas velocities at the inlet to the test section. It may be noted that, for the smooth, rough wavy or agitated section, the axial limits for $V_f > V_g$ tend to lie above the mean regression line determined for data with $V_f < V_g$; notably for the range of $We_{g,rel}/\alpha^2$ over which L_B/D_j is only susceptible to liquid conditions. It may also be noted that the above trend is most pronounced for the smooth section, with vestiges in the rough wavy and agitated regions. The clear implication here is that viewing the results solely in terms of the absolute values of relative velocity or Weber number does not provide a very accurate picture of the axial limits of the flow regimes.

Over the range where L_B/D_j is independent of $We_{g,rel}/\alpha^2$, a linear regression using only data for $V_f < V_g$ resulted in relations of the form

$$L_B/D_j \lesssim A_i\, Re_j^{-0.53}\, We_j^{0.5}. \tag{3}$$

The numerical values of the constant, A_i, together with the approximate ranges of validity of equation (3) are summarized in Table 1. From comparison of the A_i values in Table 1 with the value in equation (1), i.e. $A_i = 480$, which was developed from adiabatic tests based on the break-up mechanism of free liquid jets, it is quite apparent that equation (1) would predict lengths that are somewhat higher than, but not significantly different from, the combined lengths determined here for the smooth and rough wavy sections.

When L_B/D_j depends on $We_{g,rel}/\alpha^2$, the data are approximated by

$$L_B/D_j \leqslant B_i\, Re_j^{-0.53}\, We_j^{0.5}[We_{g,rel}/\alpha^2]^{m_i}. \tag{4}$$

The appropriate values for B_i, m_i along with the ranges of validity are also given in Table 1. The values for B_i

Table 1. Summary of predictive equations

Flow section	First region† $L_B/D_j \lesssim A_i\, Re_j^{-0.53}\, We_j^{0.5}$ A_i	Validity range for $We_{g,rel}/\alpha^2$	Second region† $L_B/D_j \leqslant B_i\, Re_j^{-0.53}\, We_j^{0.5}[We_{g,rel}/\alpha^2]^{m_i}$ B_i	m_i	Range for $We_{g,rel}/\alpha^2$
Smooth	<80	$\leqslant 10^{-2}$	25	−0.27	$>10^{-2}$
Rough wavy	<380	$\leqslant 10^{-1}$	200	−0.31	$>10^{-1}$
Agitated	<770	$\leqslant 3.5$	1500	−0.5	>3.5
Dispersed	>770	$\leqslant 10$	—	—	

† Range for Re_j and We_j: $1775 \leqslant Re_j \leqslant 13\,280$ and $4.5 \leqslant We_j \leqslant 260$.

and m_i were determined by logarithmic least squares technique and the correlation coefficients were between 0.85 and 0.9, these being as good as can be expected for carefully run experiments using a visual analysis for flow regime characterization; especially since in the case of the smooth section replicate runs sometimes resulted in lengths that differed by as much as 100%. In this regard, it is pertinent to note that the length of the smooth section rarely exceeded $2D_j$ for $V_{g,rel} \geqslant 0.5$ m s^{-1}. It may be noted that, for the constants A_i and B_i (Table 1), the last digits have been rounded to zero or five and the error introduced by this procedure is less than 1%.

4.3. *Simplified correlations*

The presentation in the preceding section is important in two respects. First, it provides good insight into the mechanisms that determine the axial extents of the various flow sections. And, second, good estimates of the critical gas Weber number for transition, from regions with no effect to those with marked dependence on relative velocity, can be established for nearly all of the flow sections.

For low-to-moderate gas velocities satisfying the conditions $V_g - V_f > 0$ and $L_B/D_j = f(Re_j, We_j)$, a further simplification of equation (3) can be made in order to provide predictive equations that may be readily applied for design calculations. Realizing that $We_j/Re_j = \mu_f V_f/\sigma_f$ (=capillary number, Ca_j), equation (3) can be re-written as

$$(L_B/D_j)\, Re_j^{0.5}\, We_j^{-0.5} = (L_B/D_j)\, Ca^{-0.5} < A_i/Re_j^{0.03} \tag{5}$$

or

$$L_B/D_j \leqslant C_i(We_j/Re_j)^{1/2} \leqslant C_i\sqrt{Ca_j}. \tag{6}$$

A straightforward re-analysis of the data for each trial was carried out by dividing the already computed A_i values by $Re_j^{0.03}$. For the $1.774 \leqslant Re_j \leqslant 13\,279$ range covered in the present study, $Re_j^{0.03}$ varied from 1.252 to 1.330, with an average value which could be stated as 1.296 ± 0.034, i.e. with about a 3% variation about the mean value. Although a very good estimate of the constant C_i for each flow section can be obtained by simply dividing the appropriate value in Table 1 by 1.296, a linear regression using the new data set resulted in the following correlations:

smooth section:

$$L_B/D_j \leqslant 60\sqrt{Ca_j}, \quad \text{for } (We_{g,rel}/\alpha^2) \leqslant 10^{-2} \tag{7}$$

rough wavy section:

$$L_B/D_j \leqslant 295\sqrt{Ca_j}, \quad \text{for } (We_{g,rel}/\alpha^2) \leqslant 10^{-1} \tag{8}$$

agitated section:

$$L_B/D_j \leqslant 595\sqrt{Ca_j}, \quad \text{for } (We_{g,rel}/\alpha^2) \leqslant 3.5 \tag{9}$$

dispersed section:

$$L_B/D_j > 595\sqrt{Ca_j}, \quad \text{for } (We_{g,rel}/\alpha^2) \leqslant 10. \tag{10}$$

In addition to the individual ranges specified above, equations (7)–(10) are valid for $0.0028 \leqslant Ca_j \leqslant 0.02$. As with Table 1, the last digit is rounded to zero or five. Equations (7)–(9) give estimates that are close to the values observed experimentally, with a 6–20% error band. As might be expected from the trend in Fig. 4, the largest percentage differences were calculated for the relatively short smooth section.

A final comment here deals with equation (10) which might appear at first to exclude the presence of a dispersed section over a third of the initial heated portion of the test section. Of the numerous trials with $V_{rel} \leqslant 2$ m s^{-1}, about 80% of the measured lengths satisfied equation (10). For all test trials with $V_{rel} > 2.0$ m s^{-1}, equation (10) did not apply. For instance, for two nitrogen trials with $V_{rel} = 7.6$ and 5.0 m s^{-1}, the onset of a dispersed ligament/droplet section was observed to occur at about 10–13 jet hole diameters downstream from the nozzle exit, which is considerably less than about 34 diameters that could be inferred from equation (10). This continual depletion of the liquid core into ligaments/droplets of liquid with increasing relative velocity, a generally expected trend, is qualitatively in agreement with the observations of Laverty and Rohsenow [8].

4.4. *Droplet generation and drop size distributions*

Downstream of the rough wavy section, a significant portion of the liquid surface area consists of small droplets formed by roll-wave entrainment and by jet instability within the agitation region. These droplets were quite small, with sizes under 200 μm in diameter. In the immediate vicinity of the heated wall, these small droplets were probably short-lived due to very rapid vaporization.

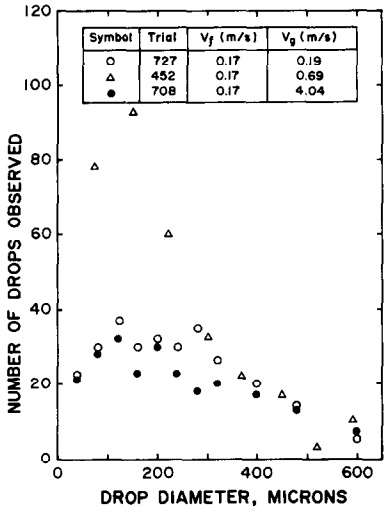

FIG. 8. Size distribution for droplets from roll-wave/agitated surface.

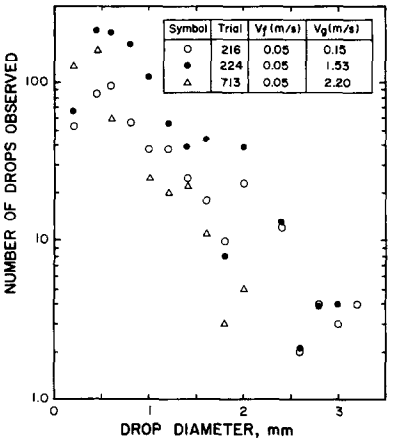

FIG. 9. Size distribution for droplets in the dispersed flow regime.

Typical size distributions for droplets formed by roll-wave entrainment and by instability at the rough surfaces of the agitated region are shown in Fig. 8 for three trials, two (708 and 727) with helium and the other with nitrogen. To obtain these data, photographs taken with the 200 mm lens (resolution down to roughly 25 μm, but limited depth of focus) focused at the depth corresponding to the outer (facing) surface of the liquid nozzle were analyzed. With this focusing, droplets within 2–3 mm of the heated wall nearest to the camera were in sharp focus. Droplets observed shearing from roll-wave crests or within 10 mm of the leading (downstream) edges of the agitated masses were measured, provided they were within sharp focus, the others being ignored.

For high, positive relative velocity $(V_g - V_f)$, the flow field near the exit of the test section is characterized by dispersed droplets, with unstable and distorted liquid ligaments/slugs for moderate relative velocities. These droplets are largely the result of roll-wave entrainment and jet instabilities, and the maximum drop size depends on the stability of the liquid core remnants and liquid mass in the agitated region. Typically, droplets/slugs over 3 mm were observed to be quite distorted and far from being spherical, a possible indication that these large drops (or small slugs) were unstable and would eventually disintegrate into smaller droplets in a sufficiently long test section.

Typical drop size distributions in the dispersed flow region are given in Fig. 9 for three trials, two (216 and 224) with nitrogen and the other with helium. These data were obtained by analyzing still photographs taken with the 55 mm lens (resolution down to about 100 μm). Spherical or near spherical droplets were recorded by diameter while unstable, distorted slugs were measured along long and short axes, and recorded by estimated total volume, assuming cylindrical form with the short axis corresponding to the diameter. For trials 216 and 224, the data are based on the analysis of two frames for $L = 40$–70 and 30–60 cm, respectively, while, for the data of trial 713, a single frame was analyzed and the distance extended from 65 to 95 cm.

The following comment can be made about the results in Figs. 8 and 9. The maximum droplet size generated at the roll-wave crests/agitated surfaces as well as droplet size distributions in the dispersed film boiling regime should depend on the gas and liquid physical properties and on the relative velocity. In view of the rather complicated nature of the droplet size dependence on these parameters, combined with knowledge that smaller droplets are short lived due to vaporization, no definite conclusions concerning these effects can be made from the limited information available.

5. CONCLUDING REMARKS

A visualization study of a simplified film boiling flow geometry, consisting of a Freon 113 liquid jet surrounded by a gas annulus, was carried out with the objective of determining the various flow regimes. It has been established that the axial flow pattern for this model of an inverted annular flow consists basically of four regions; namely, a nearly smooth section which begins at the nozzle exit, a rough wavy section with an intact liquid core, an agitated and a dispersed flow region, the latter being confined to the region near the exit of the test section. The axial limits of these flow regimes depend markedly on the relative velocity between the gas and the liquid. The axial extent of each flow zone (L_B), expressed in terms of the liquid jet nozzle diameter (D_j) as L_B/D_j, has been correlated using the liquid jet Reynolds and Weber numbers (Re_j and We_j, respectively), and a modified gas Weber number based on relative velocity ($We_{g,rel}/\alpha^2$), where α is the void fraction.

Typical size distributions for droplets generated at the roll-wave crests (the maximum size being about

500 μm) as well as those formed in the dispersed flow regime (0.5–3 mm in diameter) have been presented.

Acknowledgements—This work was performed under the auspices of the U.S. Nuclear Regulatory Commission. The authors would like to express their sincere appreciation to Drs Richard Lee and Novak Zuber for valuable discussions and support on the subject. N. T. Obot was supported as a Faculty Research Participant by the Argonne Division of Educational Programs.

REFERENCES

1. D. P. Jordan, Film and transition boiling, *Adv. Heat Transfer* **5**, 55–128 (1968).
2. L. D. Clemments and C. P. Colver, Natural convection film boiling heat transfer, *Ind. Engng Chem.* **62**(9), 26–46 (1970).
3. E. K. Kalinin, I. I. Berlin and V. V. Kostyuk, Film-boiling heat transfer, *Adv. Heat Transfer* **11**, 51–197 (1975).
4. J. W. H. Chi and A. M. Veterc, Two-phase flow during transient boiling of hydrogen determination of non-equilibrium vapour fractions, *Adv. Cryogen. Engng* **9**, 243–253 (1964).
5. J. W. H. Chi, Cooldown temperatures and cooldown time during mist flow, *Adv. Cryogen. Engng* **10**, 330–340 (1965).
6. J. W. H. Chi, Slug flow and film boiling of hydrogen, *J. Spacecr. Rockets* **4**(10), 1329–1332 (1967).
7. E. K. Kalinin, V. K. Koshkin, S. R. Yarkho, I. I. Berlin, Y. S. Kochelaev, V. V. Kostyuk, A. L. Kurolev and G. N. Sdobnov, Investigation of film boiling in tubes with subcooled nitrogen flow, *Proc. 4th Int. Heat Transfer Conf.*, Paper B.4.5, Paris (1970).
8. W. F. Laverty and W. M. Rohsenow, Film boiling of saturated nitrogen flowing in a vertical tube, *ASME J. Heat Transfer* **89**, 90–98 (1967).
9. R. P. Forslund and W. M. Rohsenow, Dispersed flow film boiling, *ASME J. Heat Transfer* **90**, 399–407 (1968).
10. G. DeJarlais, An experimental study of inverted annular flow hydrodynamics utilizing an adiabatic simulation, Argonne National Laboratory Report ANL-83-44, NUREG/CR-3339 (1983).
11. G. DeJarlais, M. Ishii and J. Linehan, Hydrodynamic stability of inverted annular flow in an adiabatic simulation, *Trans. ASME J. Heat Transfer* **108**, 84–92 (1986).
12. M. Ishii and G. DeJarlais, Flow regime transition and interfacial characteristics of inverted annular flow, *Nucl. Engng Des.* **95**, 171–184 (1986).
13. G. DeJarlais and M. Ishii, Inverted annular flow experimental study, Argonne National Laboratory Report ANL-85-31, NUREG/CR-4277 (1985).
14. M. Ishii and G. DeJarlais, Flow visualization study of inverted annular flow of post dryout heat transfer region, *Proc. 3rd Int. Topical Mtg on Reactor Thermal Hydraulics*, Paper 1.C, Newport, Rhode Island (1985).
15. M. Ishii and G. DeJarlais, Flow visualization study of inverted annular flow of post dryout heat transfer region, *Nucl. Engng Des.* **99**, 187–199 (1987).
16. R. W. Graham, R. C. Hendricks, Y. Y. Hsu and R. Friedman, Experimental heat transfer and pressure drop of film boiling liquid hydrogen flowing through a heated tube, *Adv. Cryogen. Engng* **6**, 517–524 (1961).
17. P. Ottosen, Experimental and theoretical investigation of inverse annular film flow and dispersed droplet flow, important under LOCA conditions, Riso National Laboratory Report No. R-424, Denmark (1980).
18. A. A. Kurilenko, S. R. Dymenko and Yu. S. Kochelaev, Phase slip and heat transfer to the liquid in film boiling of a cryogenic liquid in piston flow, *J. Engng Phys.* **39**, 961–965 (1981).
19. I. Vojtek, Investigation of dispersed flow heat transfer using different computer codes and heat transfer correlations, *Proc. 1st Int. Workshop on Fundamental Aspects of Post-dryout Heat Transfer*, NUREG/CP-0060, Salt Lake City, Utah, 2–4 April (1984).
20. S. W. Webb and J. C. Chen, A two-region vapor generation rate model for convective film boiling, *Proc. 1st Int. Workshop on Fundamental Aspects of Post-dryout Heat Transfer*, NUREG/CP-0060, Salt Lake City, Utah, 2–4 April (1984).
21. D. C. Groeneveld, Inverted annular and low quality film boiling: a state-of-the-art report, Keynote Paper, *Proc. 1st Int. Workshop on Fundamental Aspects of Post-dryout Heat Transfer*, NUREG/CP-0060, Salt Lake City, Utah, 2–4 April (1984).
22. J. C. Chen, Review of post-dryout heat transfer in dispersed two-phase flow, Keynote Paper, *Proc. 1st Int. Workshop on Fundamental Aspects of Post-dryout Heat Transfer*, NUREG/CP-0060, Salt Lake City, Utah, 2–4 April (1984).
23. G. Yadigaroglu and A. Bensalem, Interfacial mass generation rate modeling in non-equilibrium two-phase flow, *Proc. Int. Workshop on Two-phase Flow Fundamentals*, Gaithersburg, Maryland, 22–27 September (1985).
24. Ye. N. Sinitsyn, G. W. Muratov and V. P. Skripov, The surface tension of F-11, 21 and 113, *Heat Transfer—Sov. Res.* **4**(4), 79–80 (1972).
25. M. Ishii and M. A. Grolmes, Inception criteria for droplet entrainment in two-phase concurrent film flow, *A.I.Ch.E. Jl* **21**(2), 308–317 (1975).
26. N. T. Obot and M. Ishii, Two-phase flow regime transition criteria in post-dryout region based on flow visualization experiments, Argonne National Laboratory Report ANL-87-27, NUREG/CR-4972 (1987).

CRITERE DE TRANSITION DU REGIME D'ECOULEMENT DIPHASIQUE DANS LA REGION APRES ASSECHEMEMENT, D'APRES DES EXPERIENCES DE VISUALISATION D'ECOULEMENT

Résumé—On conduit une étude de visualisation de l'ébullition en film pour déterminer le critère de transition du régime d'écoulement dans la région après la zone critique. Un écoulement annulaire inversé, idéal, est obtenu en introduisant un jet liquide de Freon 113 à travers une tuyère, centré avec précision sur un écoulement annulaire de gaz. Les domaines respectifs des vitesses de liquide et de gaz sont 0,05–0,5 et 0,03–8,2 m s^{-1}. On utilise l'azote et l'hélium. Dans la présente configuration, on considère quatre régimes d'écoulement : l'écoulement annulaire inversé lisse, le régime rugueux de vagues, le régime agité et le régime dispersé.

KRITERIEN FÜR STRÖMUNGSFORMÜBERGÄNGE IM POST-DRYOUT-GEBIET AUFGRUND VISUELLER BEOBACHTUNGEN

Zusammenfassung—Zur Bestimmung von Kriterien für die Strömungsformübergänge im Post-Dryout-Gebiet werden visuelle Beobachtungen beim Filmsieden durchgeführt. Eine ideale inverse Ringströmung wird dadurch erhalten, daß ein Strahl flüssiges R113 durch eine Düse in eine Ringströmung aus Gas eingebracht wird. Der Strahl ist dabei genau zum Innendurchmesser der Meßstrecke zentriert. Die Geschwindigkeitsbereiche für Flüssigkeit und Gas betragen 0,05–0,5 bzw. 0,03–8,2 m s^{-1}. Es wird Stickstoff und Helium verwendet. Vier Strömungsformen wurden bei der vorhandenen Konfiguration festgestellt: eine glatte und eine wellige inverse Ringströmung, sowie eine aufgewirbelte und eine disperse Strömungsform.

КРИТЕРИИ ПЕРЕХОДА ДЛЯ ДВУХФАЭНОГО РЕЖИМА ТЕЧЕНИЯ В ЭАКРИТИЧЕСКОЙ ОБЛАСТИ, ОСНОВАННЫЕ НА ЭКСПЕРИМЕНТАХ ПО ВИЭУАЛИЭАЦИИ ПОТОКА

Аннотация—Проводено виэуальное исследование пленочного кипения с делью определения критериев перехода для режима течения в области критического теплового потока. Посредством введения струи жидкого фрсона 113 с кольцевым потоком газа черсэ сопло, расположенное строго в центре внутреннего диаметра исследуемого участка, получен идеализированный обращенный кольцевой поток. Диапаэоны скоростей жидкости и газа соответственно составляют 0.05–0.5 и 0.03–8.2 м/с. Исследования проводились с аэотом и гелием. Для данной конфигурации установлено четыре режима течения, а именно длавный участок обращенного кольцевого потока, волнообраэный, перемешанный и дисперсный режимы течения.